



OPEN

SUBJECT AREAS:

OPTOFLUIDICS

BIOSENSORS

NANOPHOTONICS AND
PLASMONICSCHARACTERIZATION AND
ANALYTICAL
TECHNIQUES

Surface-enhanced molecular spectroscopy (SEMS) based on perfect-absorber metamaterials in the mid-infrared

Yongqian Li¹, Lei Su¹, Chen Shou¹, Chunmeng Yu², Jinjun Deng¹ & Yu Fang²¹Key Laboratory of Micro/Nano Systems for Aerospace of Ministry of Education, Northwestern Polytechnical University, Xi'an, China, 710072, ²School of Chemistry and Materials Science, Shaanxi Normal University, Xi'an, China. 726001.Received
24 April 2013Accepted
17 September 2013Published
4 October 2013Correspondence and
requests for materials
should be addressed to
Y.L. (liyq@nwpu.edu.
cn)

Surface-enhanced infrared absorption spectroscopy has attracted increased attention for direct access to molecular vibrational fingerprints in the mid-infrared. Perfect-absorber metamaterials (PAMs) with multi-band spectral responses and significant enhancement of the local near-field intensity were developed to improve the intrinsic absorption cross sections of absorption spectrum to identify the vibrational spectra of biomolecules. To verify its performance, the proposed infrared PAM array was used to identify the molecular stretches of a Parylene C film. The resonant responses of the infrared PAMs were accurately tuned to the vibrational modes of the C=C target bonds. The vibrational stretches of the C=C moiety were observed and the auto-fluorescence mechanisms of the Parylene C film were monitored. The unique properties of the PAMs indicate that this approach is a promising strategy for surface-enhanced molecular absorption spectroscopy (SEMS) in the mid-infrared region and for the tracking of characteristic molecular vibrational modes.

Increasing requirements for single-molecule identification are emerging for public applications¹, in areas such as health care², the monitoring of trace elements in the environment and water/food safety; these requirements constantly push the development of detection modalities aimed at the detection of rare target analytes with ultra-sensitive precision, specificity and multiplex capabilities³. Various devices and systems have achieved the integration and miniaturization required for multiplex detection and sensitivity improvements⁴. These methods are based on electrical, magnetic and mechanical principles and optical strategies such as optical waveguides⁵, surface plasmon waveguides and optical resonators^{6,7}. These methods are significantly advantageous for real-time monitoring in biology and have enabled numerous experiments and biochemical investigations^{4,8}. The specificity for and multiplex detection of target molecules are achieved through chemical functionalization of the device surface⁹ or are typically performed by devices⁴.

The unusual optical properties of the emergent nanostructure arrays present another label-free methodology. Surface plasmon resonance (SPR)^{10,11} and localized surface plasmon resonance (LSPR)^{12,13} have become recognized as 'gold standard' biosensing techniques^{14,15}. Extraordinary optical transmission (EOT) of sub-wavelength plasmonic nanohole arrays enables high-throughput multiplex detection with a small sensor volume¹⁵⁻¹⁷. The ability to tailor the electromagnetic wave of the metamaterials has expanded the sensitivity and multiplex capabilities into the area of biochemical interactions¹⁸ and has encouraged the emergence of surface-enhanced molecular spectroscopies^{19,20}. Infrared absorption spectroscopy enables direct access to the vibrational fingerprints of a molecular structure, but due to the intrinsic absorption cross section of the active molecular excitation in infrared absorption spectroscopy, the sensitivity is still much lower than that of fluorescence label-based methods²¹. Plasmonic nanoantennas have been excited to demonstrate the direct detection of vibrational signatures of single protein monolayers. The vibrational spectra of proteins have been obtained at zeptomolar levels corresponding to hundreds of molecules per antenna¹⁹. The asymmetric resonance of a Fano-resonant metamaterial has a sharper spectral response and higher field enhancement to serve as a platform for multispectral biosensing to recognize proteins²² and to detect the chemical binding of target antibodies²³. The commonly used amide vibrational peaks of proteins require resonance quality factors Q greater than 10^{22} . Most plasmonic metamaterials are unable to attain such rigorous resonant lines at infrared frequencies. Additionally, a narrower



linewidth implies a larger field enhancement over the surface of a planar plasmonic metamaterial. However, transmitting metamaterials provide neither field confinement nor specific narrow responses because of their poor collective resonances.

Fortunately, the recently emerging perfect-absorber metamaterials (PAMs) exhibit strong local electromagnetic concentration and narrow spectral tunability resulting from matter-photon interactions. Near-field plasmonic enhancement of the absorption of PAMs has been demonstrated with a metal-dielectric-metal structure²⁴, in which the resonance response can approach unity in certain frequency regions^{25–27}. The intrinsic spectral sensitivity of PAMs to small perturbations in their geometries facilitates the tunability of the resonance spectrum. Additionally, the dramatic dependence of the line-shape shifts on the local environment improves the detection limit in biosensing^{28,29}. For mid-infrared spectroscopy, this property is significant because various biological moieties are characterized by multiple vibrational fingerprints. The mid-infrared response characteristics of the surface-enhanced perfect absorption enable the implementation of precision identification of individual molecular species and can even enable the detection and characterization of complex biological molecular regions, thereby improving the specificity of biodetection³⁰. In particular, the plasmonic resonances of PAMs can be tuned to certain spectral regions of interest with tolerant spatial reproducibility.

The advantages of multiple-band absorption and intuitive tunability make PAMs particularly attractive for the development of a new generation of label-free mid-infrared molecular absorption spectroscopies³² and make it possible to approach the detection limit for single-molecule binding events³³. Efficient perfect-absorption sensing has been performed for an asymmetric 'H' structure, in which the resonance of the electromagnetically induced transparency (EIT)³⁴ is sensitive to the presence of glucose in an aqueous solution around each sensing element. This asymmetric geometry exhibits high detection sensitivities of 600 nm per refractive-index unit³². Three widely separated molecular vibrational modes of C=O and C-H in a thin film of PMMA were revealed using a carefully designed plasmonic PAMs³¹. Particularly in mid-infrared spectroscopy, dual- or multi-band perfect absorbers have been designed to explore the structural diversity of two molecular stretches of polymer films^{35,36}; these absorbers have potential for various applications, such as the simultaneous monitoring of multiple fingerprint characteristics during structural transformation and the dissimilarity between different molecular regions^{21,23,37}. Although these achievements only cover part of the mid-infrared range¹⁹, they have the potential to be readily achieved for arbitrary frequency segments for implementing molecular absorption spectroscopy in the mid-infrared region with multi-band responses and surface enhancement, with the goals of sensitivity, specificity and multiplex detection^{17,38,39}.

To achieve surface-enhanced multi-band infrared spectroscopy, a perfect-absorber metamaterials array was developed; in this array, cross-shaped perfect absorbers were arranged in diagonal patterns. We first tailored the geometry of individual PAMs array to form resonant structures that match the molecular vibrational modes of interest. The array was specifically designed to attain multiple-wavelength spectral resonances in the mid-infrared region. The amplitudes and resonant frequency shifts at two frequency bands were tuned to match the molecular vibrational modes of the analyte and to maximize the enhancement and accuracy for the analyte. The molecular vibrational modes of the C=C bond in thin films of Parylene C were revealed through the absorption difference spectra for the developed PAM arrays. The surface enhancement and multiplex spectral response in the mid-infrared region make this platform a powerful and versatile technology for ultra-sensitive molecular vibrational spectroscopy¹⁷.

Results

Cross-shaped perfect-absorber arrays and multi-band absorption spectrum. A concept schematic of the embedded PAMs on the surface of the substrate chip is shown in figure 1 (a). The real

device is one chip measured using an Fourier-transform infrared spectrometer (FTIR) equipped with an infrared microscope. The device consists of a few square detection regions with elaborately designed PAM arrays. One of cross-shaped PAMs array is shown in figure 1 (b), in which the inset gives the arrays of cross-shaped nanoresonators arranged in diagonal pattern. A molecular film of Parylene C, tens of nanometers in thickness, was chosen as a sample analyte to coat the PAM. Then the FTIR is used to measure the absorption response. The absorption responses before and after coating are used to identify the existing of molecule.

The PAM arrays were deliberately designed to induce distinct resonances through the surface-enhanced perfect absorption. The resonance wavelength was strongly dependent on the occurrence and the concentration of the analyte in the adjacent medium around the metallic nanostructure, as shown in figure 1 (c). A single unit of an infrared PAM, which is a typical metal-insulator-metal absorber structure, as shown in figure 2 (a), consists of a metallic cross-shaped nanoresonator on top of a barrier film above a ground plane deposited on a silicon substrate. The array of metallic nanoresonators and the ground plane film are separated by a thin Al₂O₃ film. The array of cross-shaped nanoresonators plays a role similar to that of an electric ring resonator (ERR)⁴⁰, which strongly manipulates the incident electromagnetic wave. Compared to the arrays of cross-shaped PAMs investigated in the previous literature^{28,41,42}, the diagonal patterns provide two bands and sharper spectral responses in the mid-infrared region. The electric response can be tuned by altering the sizes of the cross-shaped resonators, and the magnetic response can be tuned by the thickness of the dielectric layer between the resonator arrays and the ground plane^{43–45}. At specific frequencies, impedance-matching conditions are met for the nanoresonator array and the surrounding medium, and these conditions result in a maximized narrow-band absorbance.

To identify an infrared molecular fingerprint, one must be able to easily position the resonance response throughout the mid-infrared. This capability is demonstrated in figure 2 (b), which shows the resonance tunability of the PAM structure for different values of the arm length *L*. As the arm length *L* increases, the associated resonant mode becomes red-shifted. The absorption spectra of the PAM structure measured are in close agreement with numerical simulations. The resonance response at short wavelengths (M2) is attributed to the propagation surface plasmons (SPPs) excited at the interface through a coupling mechanism⁴⁶. The mode M1 is red-shifted as the distance between the two arms increases and exhibits characteristics typical of surface plasmon resonance. The linear sensitivity relationship has been observed previously and can be explained by circuit theory⁴⁷. The resonant absorption peaks are primarily sensitive to the arm lengths of the PAM structure, although other geometric factors contribute slightly to the resonance. The displayed resonance tunability is highly advantageous for surface-enhanced measurements in the infrared region^{48,49}.

Local field enhancement by collective resonances. In this work, we aimed to engineer PAMs that support spectrally narrow collective plasmon excitations at mid-infrared frequencies, specifically at the amide vibrational peaks of the protein, which fluctuate from 1620 cm⁻¹ to 1680 cm⁻¹ (amide I) and 1510 cm⁻¹ to 1580 cm⁻¹ (amide II), and the vibrational normal modes of the polymer sample. The lithographically fabricated structures are then coated with a monolayer of the polymer, and the vibrational dipole moments of the molecules act as a load for the PAM resonators. Nanoresonator arrays, driven by an infrared resonance source, efficiently focalize the incident wave to the load through the collectively enhanced plasmonic excitations.

Under resonant absorption conditions, the nanostructure arrays efficiently tailor the incident electromagnetic wave through the enhanced plasmonic excitations⁴⁶. For an individual cross-shaped

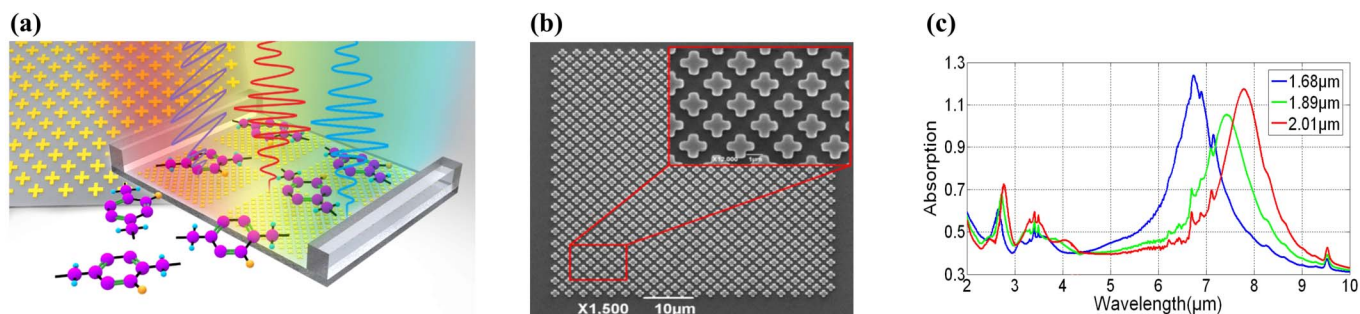


Figure 1 | (a) Schematic of the architecture of the conceived device with the embedded perfect-absorber metamaterial (PAM) array. A few PAMs arrays were designed and fabricated in the substrate chip. A Parylene C molecular film was chosen as an example. Beams of incident and reflect light are used to measure the absorption response by FTIR. PAMs array is shown in background. (b) A typical scanning electron microscopy image of the fabricated PAM array and the geometric sizes. A magnified image of the device is shown in the insert. (c) The resonance spectra of three PAM samples coated with Parylene C film; in these spectra, the molecular vibrational stretches can be observed.

perfect absorber, the EM wave response is controlled by the incident field that excites the localized surface plasmons (LSPs) serving as the electric dipoles. However, for an array, the resonance responses are attributed to not only the single excitations induced by the incident electromagnetic field but also to the induced scattered fields from the dipoles of the other nanoresonators. The local electromagnetic fields around the i^{th} nanoparticle are created by the incident electromagnetic fields and the other induced dipole fields.

$$E_{L,i} = E_{Inc,i} + E_{Ind,i} = E_0 e^{ikr_i} + \sum_{i \neq j} c_{ij} P_j e^{ikr_{ij}} \quad (1)$$

where E_0 and $k = 2\pi/\lambda$ are the amplitude and the wave vector of the incident wave. P_j is the induced polarization of the j^{th} resonator in the array. The c_{ij} values represent the dipolar interaction between the nanoparticles without the phase term¹⁹. If the induced dipolar field interactions within the array patterns are almost in phase, the local fields satisfy the resonance oscillation and become extremely large. Therefore, in an array of perfect absorbers in phase, the extremely localized field redistribution results in strongly enhanced near-field excitation.

For normal incident light at the nanoresonator array, previous simulations showed that the near-field intensities were enhanced by a factor of 10^2 – 10^3 ⁵⁰. Although these enhancement factors are quite impressive, higher near-field intensities are required for monolayer molecular measurements. In the array structure, hybrid excitations in well-engineered perfect-absorber ensembles can be exploited to achieve dramatically enhanced near-field intensities with much

narrower far-field spectral responses. As shown in figure 3 (b), the near-field enhancement of the Poynting field ($|P|^2$) in the cross-sectional plane of the PAM was computed by three-dimensional FDTD simulations at excitation wavelengths of 6.40 μm and 2.275 μm . The simulations indicated that the electromagnetic energy was efficiently confined in the Al_2O_3 spacer layer and that a locally enhanced electromagnetic field was established at the gaps and tips between adjacent nanoantenna resonators. The largest Poynting intensity enhancement of 10^4 – 10^5 was obtained at the tips of the cross-shaped nanoantennas. The large spectrally selective enhancement holds promise for sensing applications, as demonstrated below.

Optical constants and the spectra of Parylene C film. As a proof of concept, Parylene C film was chosen as a model system to prove the mechanisms of the infrared surface enhancement spectroscopy. Parylene has exceptional mechanical and optical properties for nanostructures^{43,51}. Additionally, it has several well-known characteristic absorption bands in the infrared range. The absorption bands of the C-H and C=C molecular stretches are dependent on the dehydrogenation and oxidation processes that occur in long-duration illumination⁴³.

First, the absorption spectral properties of a Parylene C film evaporated on a bare substrate were measured as displayed in figure 4 (a). There are three distinct absorption peaks in the infrared range at 3.29 μm (3031.8 cm^{-1}), 6.89 μm (1450.3 cm^{-1}) and 9.57 μm (1044.9 cm^{-1}). The optical constants in the mid-infrared were also measured as shown in figure 4 (b), which agrees well with the absorption spectral positions. The optical constants below give reasonable

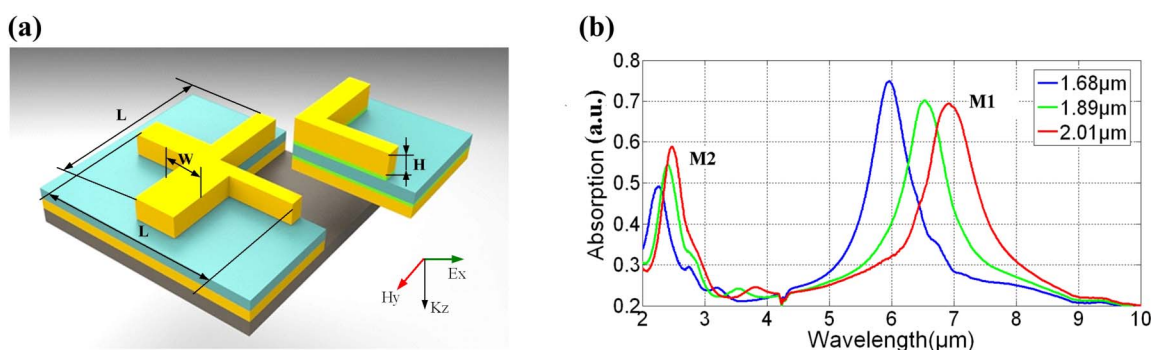


Figure 2 | Schematic of the perfect-absorber metamaterials (PAMs) and the tunability of their resonance spectra. (a) One PAM unit cell and the corresponding structural parameters. The cross-sectional view displays the layers, including the barrier layer of gold, the dielectric spacer layer of Al_2O_3 and the topmost gold antenna. Two thin layers of titanium material are included to improve adhesion between the layers. The parameters of the designed PAMs are characterized by the arm length (L), the arm width (W) and the length of the periodic region (P). The thickness of the topmost gold layer of the nanoantenna is labeled H . (b) The resonance response spectra as a function of the arm length L ; the resonance peaks become red-shifted as the arm length increases.

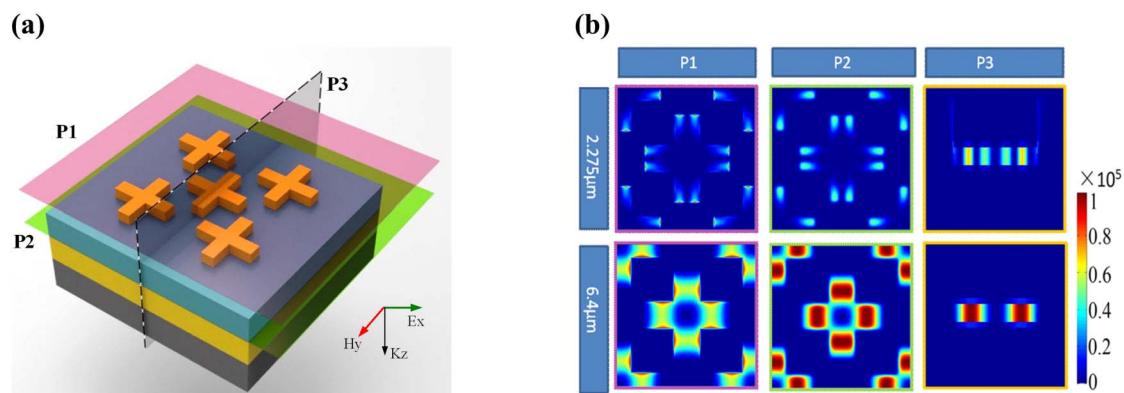


Figure 3 | Near-field Poynting field ($|P|^2$) distribution, which manipulates the infrared absorption spectrum at the resonant wavelengths of 6.40 μm and 2.275 μm . (a) Three-dimensional view of the simulated absorber structure. Cross section P1 is along the X-Y plane located at the top surface of the Au resonator array (pink plane), and the monitoring cross section P2 for the simulation is along the bottom dielectric $\text{Al}_2\text{O}_3/\text{Au}$ layer (green plane). The sectional monitor P3 (grey plane) transects one cross-shaped resonator (grey plane). (b) The enhancement factor for the field distribution over the tips of the perfect absorber shows the confinement and redistribution of electromagnetic energy. The color bar shows the enhancement factor.

results. The strong peaks at approximately 1450.3 cm^{-1} ($6.89\text{ }\mu\text{m}$) correspond to the C=C stretch. The side lobes of the peaks at $6.89\text{ }\mu\text{m}$ (1450.3 cm^{-1}) are an asymmetric minor absorption and indicate the presence of substituent groups. The peak at approximately $9.57\text{ }\mu\text{m}$ (1044.9 cm^{-1}) arises from the small number of C-Cl stretches. The small peak at $3.29\text{ }\mu\text{m}$ (3031.8 cm^{-1}) corresponds to the vibrational stretches of the C-H group. The data agree well with the vibrational reflection dips reported in the mid-infrared⁴³, although the spectra of the vibrational bonds are slightly displaced from their typical positions because of the illumination duration.

Based on the optical constant results shown in figure 4, the infrared absorption spectra of the PAMs before and after coating with Parylene C film were studied. The presence of the thin polymer film changes the dielectric environment of the PAMs and results in frequency shifts. The complex value of the frequency shifts affects both the spectral position (index-induced shift) and the surface-enhanced absorption²³. The refractive index of Parylene C contains a nondispersive component of $n = 2.5$, as indicated in figure 4 (b); this component induces a frequency shift in the resonance response of the PAM. The frequency shifts scale with the thickness of the film; this result was verified by numerical simulations and experiments. The spectral difference before and after the coating process was calculated, as shown in figure 5 (b). The inset chart indicates the

linear relation between the frequency shift of the peak and the thickness of the polymer for films less than tens of nanometers thick; this relation allows the polymer thickness to be estimated³¹. Analogous to the figure of merit (FOM) for the refractive index sensitivity measurements⁵², the function for assessing the sensing potential is defined by

$$FOM = \frac{m(eV\ T^{-1})}{fwhm(eV)} \quad (2)$$

where T represents the thickness and m is the linear regression slope in figure 5 (b) for the thickness dependence. This definition allows nanostructures to be judged against one another as sensing platforms, independent of the shapes or sizes of the nanostructures. The FWHM of each of the three resonant spectra in figure 5 (a) were represented in terms of energy (eV). The result of 1.79 shown in figure 5 (b) indicates the significant sensitivity of surface-enhanced molecular spectroscopy based on PAMs.

Detection of the molecular vibrations of Parylene C film. We focus our attention on the information in the molecular stretches. The Parylene C films with varying thicknesses were evaporated on a bare substrate and on the surface of the PAMs with a film coating system (Specialty Coating System, Inc.). The infrared absorption

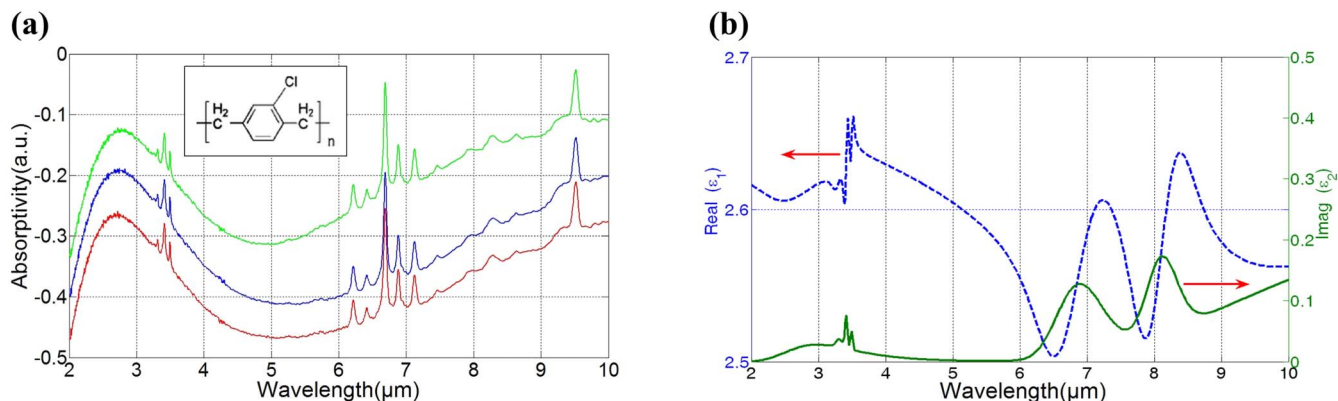


Figure 4 | The optical properties of Parylene C film in the mid-infrared region from 2.0 μm to 10.0 μm . (a) The absorption spectrum measured by FTIR spectrometry of Parylene C film with a thickness of less than $0.80\text{ }\mu\text{m}$. The repeating unit of the Parylene C polymer is shown in the inset. Three measurements were repeated for Parylene C films with slightly different thicknesses. The obvious strong absorption bands correspond to the vibrational stretches of C-H at approximately $3.29\text{ }\mu\text{m}$ (3031.8 cm^{-1}), C=C at $6.89\text{ }\mu\text{m}$ (1450.3 cm^{-1}) and C-Cl at $9.57\text{ }\mu\text{m}$ (1044.9 cm^{-1}). (b) The optical constant was measured by spectroscopic ellipsometry (IR-VASE®, J.A. Woollam). The permittivity of Parylene C contains a nondispersive component in the refractive index.

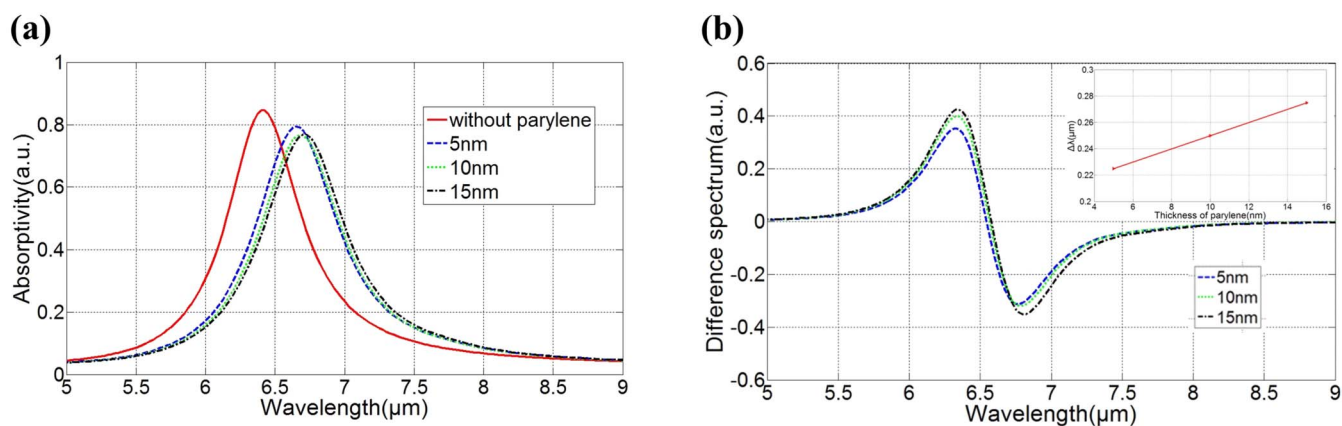


Figure 5 | PAMs manipulate the infrared absorption spectra. (a) Analytic absorption spectrum from PAMs before and after functionalization for increasingly thick Parylene C layers, for less than tens of nanometers. (b) The difference spectra calculated from the absorptivity. The nondispersive component containing the refractive index of the Parylene C contributes to the shift in the resonant frequency. The inset presents the linear relation between the wavelength and the thickness of the polymer film.

spectra before and after the Parylene C film coating were measured with a FTIR spectrometer. To obtain information on the molecular vibrational stretches, the frequency-shift method was used to eliminate the effect of the dielectric constant^{23,31}. The characteristic molecular vibrational stretches were explicitly revealed in the absorptive different spectra. The corresponding difference spectra were calculated from $\Delta A = A'_{before} - A_{after}$, where A'_{before} and A_{after} are the absorption spectra of the bare perfect-absorber array and the PAMs coated with Parylene C, respectively. The frequency-shift absorption spectra were obtained by transforming the spectral signatures of the coating with the wavelength difference $\Delta\lambda = \lambda_{before} - \lambda_{after}$ through the relation $A'_{before} \rightarrow A(\lambda_{before} - \Delta\lambda)$; this transformation was performed through a homebuilt frequency calibration program. The absorbance difference spectra estimated for two PAM arrays with different arm lengths before and after coating with Parylene C film were extracted, as shown in figure 6. The electromagnetic response of the PAM results in a slight shift in the resonant spectra and fluctuations in the light intensity. These fluctuations were normalized with a polynomial fitting procedure for the difference spectra¹⁹, $\Delta A/A_0 = (A_{before} - A_{after})/A_0$, where A_0 is the absorption signal from a reference surface. In addition to the above frequency shifts, the difference spectrum distinctly reveals the characteristic absorption bands corresponding to the C=C stretch in Parylene C at 1450.3 cm^{-1} (6.89 μm). As shown in figure 6 (b), the absorption difference spectrum for the C=C stretch shows pronounced enhancement with a narrow line width caused by both the intrinsic peaks and the superposition of the perfect spectrum with the resonance modes of the PAM arrays.

As shown in figure 6, the dashed vertical lines indicate the positions of the peaks in the absorption spectrum that result from the vibrational stretches of the C=C groups. The observed difference signal ($\Delta A/A_0$) was 20% in the periodic PAMs. The reference surface without PAM structures was measured for Parylene C films of the same thickness. Faint absorption signals were observed in the region far from the fabricated PAMs. These results verify the use of PAMs for the identification of molecular vibrational spectra.

The absorption difference spectrum in figure 6 displays another interesting result, the asymmetric Fano profile-like shape of the spectrum²². The distortion from the normal Lorentzian shape is attributed to the strong interaction between the molecular dipoles and the resonance modes of the PAMs. Both the resonance modes of the perfect absorber and the Parylene C molecular vibrational modes induce the above asymmetric spectral modifications^{53,54}. Especially when approaching the absorption maximum, the asymmetric spectra are strongly dependent on the relative positions of the perfect-absorber peak and the molecular absorption peaks. When the excitation resonance is consistent with the molecular vibrational frequencies, a clear splitting is observed, as shown in figure 7. The asymmetric properties of the absorption spectrum will improve the sensitivity for identification^{22,23}.

Autofluorescence processes of Parylene C film. Parylene C plays a significant role as a biocompatible material in microfluidic and micro total analysis system (mTAS) applications. However, the autofluorescence of Parylene C can be a major obstacle for Parylene C-based devices in applications that require sensitive fluorescence

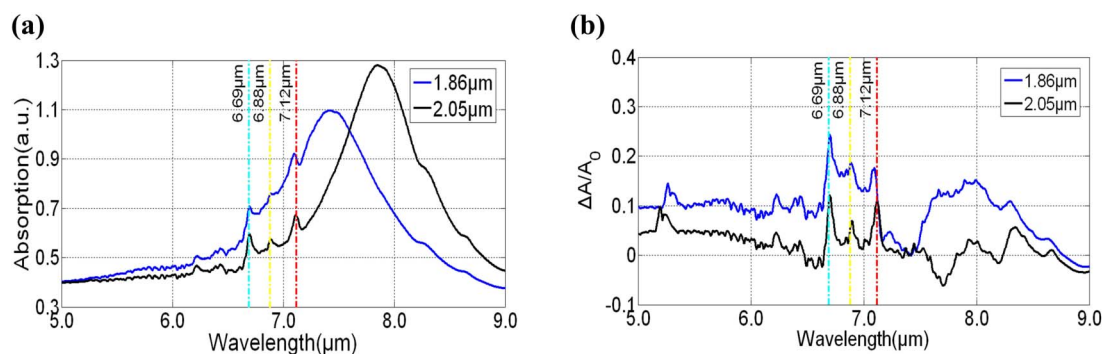


Figure 6 | Analytic and experimental absorption differences caused by the Parylene C film. (a) Absorption spectroscopy of the PAMs after coating with a thick Parylene C film. (b) Absorption difference spectra for the C=C stretches from the periodic PAMs. The characteristic vibrational stretches of the C=C group are visible in the spectra, as indicated by the vertical dashed lines. Two PAM arrays with arm lengths of 1.86 μm and 2.05 μm were measured.

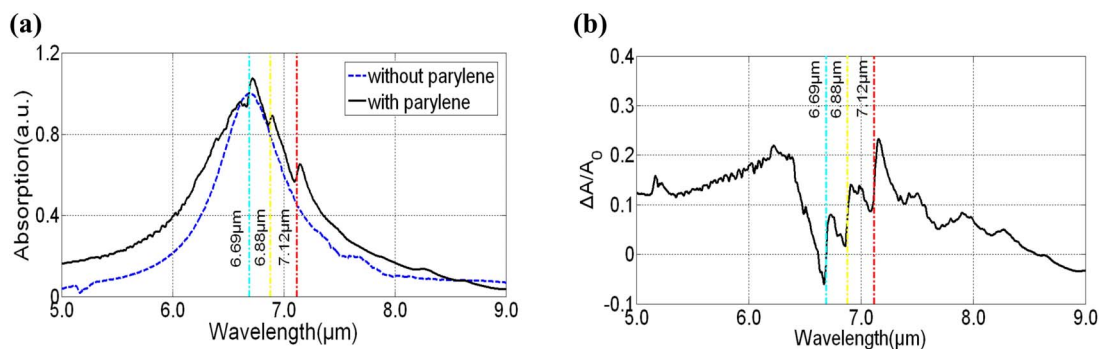


Figure 7 | The experimental asymmetric absorption difference spectrum improves the detection sensitivity. (a) The molecular vibrational stretches are well-aligned with the resonance spectra of the PAMs. (b) The absorption difference spectrum is clearly split. The dashed vertical lines indicate the positions of the absorption peaks for the C=C group in Parylene-C.

detection⁵⁵ because the autofluorescence may interfere with or even overwhelm the signals of interest, especially when UV and visible light are used for excitation⁵². For further proof of the proposed concept of PAM-based surface-enhanced molecular spectroscopy, an in-depth mechanistic description of the autofluorescence of Parylene C is given here. The Parylene C films evaporated on the PAMs were exposed to UV illumination for degeneration. At various time intervals, the spectral responses were characterized by FTIR, as shown in figure 8. As is well known, the absorption peaks from 1450–1610 cm^{-1} ($6.89 \mu\text{m} - 6.21 \mu\text{m}$) are attributed to the C=C stretching vibrations⁴³. After illumination (15 min to 60 min), the absorption peak for the C=C bonds increased. The absorption increased promptly for UV illumination durations of less than 30 minutes, whereas after longer UV illumination durations, the magnitude of the vibrational spectrum was slightly attenuated at the absorption bands, and the spectral shape and peak locations were unchanged. The above experimental results provide clues that help us to understand the maturing mechanism. The slow variation of the amplitude verifies the increasing amount of C=C bonds in the chain adjacent to the benzene ring⁴³. Some unsaturated C=C bonds in the molecular chain of the Parylene C film are generated during the evaporation and deposition process. During the initial UV illumination, the photo-oxidation of the C=C bonds was stimulated by oxygen diffusion into the film due to the permeating contact between the oxygen and carbon molecules; in addition, the unsaturated C=C defects dehydrogenated and an increasing number of C=C bonds completed the molecular chain of the Parylene C film⁵¹. After longer UV illumination times, photo-oxidation gradually became dominant. The C=C bonds in the main chain were oxidized to C-O bonds (at 1100–1300 cm^{-1} , 9.09 – 7.69 μm) or C=O bonds (approximately 1700 cm^{-1} , 5.88 μm); this oxidation resulted in the sharp reduction of the resonant magnitude indicated

in figure 8 (b). The amplitude of the absorption spectrum increased after 60 minutes at three different wavelengths: 6.69 μm , 6.88 μm and 7.12 μm , as shown in figure 8 (c).

Discussion

We have demonstrated that perfect-absorber metamaterials (PAMs) with tunable cross-shaped artificial structures can be used in surface-enhanced molecular spectroscopy (SEMS). In contrast to previous implementations of label-free methods, PAM-based infrared spectroscopy has the advantageous properties of surface plasmon-enhanced resonance and tunability of the resonance spectrum throughout the mid-infrared region. The higher local field enhancement caused by the confinement of the nanostructure increases the cross section of the infrared absorption and improves the detection sensitivity. At the same time, the tunability of the resonance spectrum enables the PAMs to match the molecular vibrational modes of interest in the analyte to identify chemical stretches. The clear observation of Parylene C molecular vibrational stretches in films with thicknesses of tens of nanometers demonstrates that the PAM-based SEMS is well suited to molecular vibrational infrared spectroscopy. Further development of multi-band PAMs can thus implement strong near-field enhancement over broadly tunable modes and can enable PAM-based SEMS to simultaneously monitor multiple chemical or biological agents or conformational changes associated with different structural stretches. This new approach of PAM-based biosensing is compatible with the lab-on-a-chip concept and offers the possibility for high-throughput analysis. Further research could exploit this method to support strong field localization for single-molecule spectroscopy.

Methods

The PAM arrays were fabricated through the standard process of sputtering and electron beam lithography (EBL) followed by lift-off⁵². Details are described in

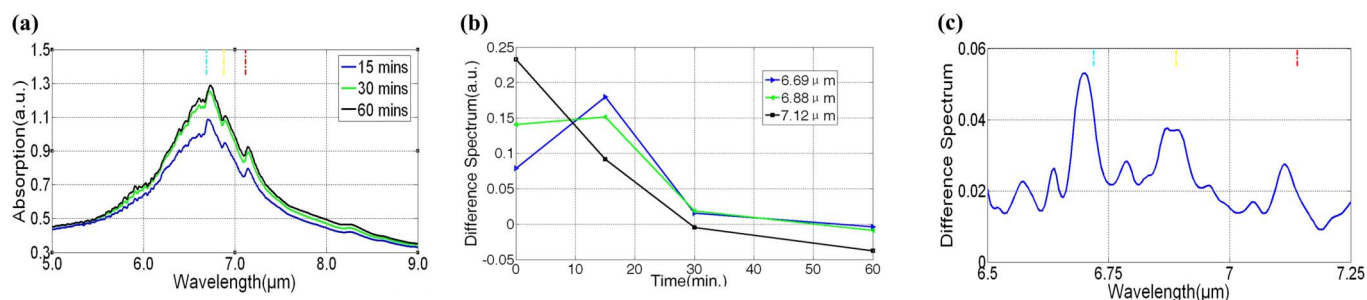


Figure 8 | The autofluorescence processes of Parylene C film under UV illumination. The variation in the C=C molecular vibrations indicates the autofluorescence mechanism. (a) The absorption spectrum of Parylene C for short UV illumination times. (b) Under UV illumination, the C=C bonds in the main chain become saturated and then oxidized; oxidation reduces the difference spectrum at three vibrational bonds. (c) The change in the absorption spectrum after 60 minutes.



Supported Information. The electromagnetic wave in the mid-infrared region from 2.0 μm to 10.0 μm was typically focused on the detection spots. The measurements were performed by mounting the biochip on an XY motorized alignment stage and by aligning the detection spots within the microscope for Fourier transform infrared (FTIR) spectroscopy with an infrared microscope. The absorption intensity and the frequency shifts were monitored before and after the analyte was placed in contact with the absorptive elements. The PAM structure was optimized using finite-difference time-domain methods (FDTD, Commercial software, Lumerical) referring to Supported Information. To obtain distinct independent resonances, the geometric parameters were scanned and optimized for the molecular vibrational bands. The thicknesses of both the upper gold film and the layer beneath the dielectric materials were chosen to be 100 nm, whereas the absorption layer of Al_2O_3 film is 50 nm thick. The transmission $T(\omega)$ and reflection $R(\omega)$ were obtained from simulations with perfectly matched boundary conditions. The frequency-dependent absorption was calculated from $A(\omega) = 1 - T(\omega) - R(\omega)$. The Parylene C films with varying thicknesses were evaporated on a bare substrate and on the surface of the PAMs with a film coating system (Specialty Coating System, Inc.). The absorption spectral properties of a Parylene C film evaporated on a bare substrate and the surface of PAMs array were measured with a Fourier transform infrared (FTIR, Vertex 70, Bruker) spectrometer. The optical constants in the mid-infrared were also measured by spectroscopic ellipsometry (IR-VASE[®], J.A. Woollam). The infrared absorption spectra before and after the Parylene C film coating were measured with a FTIR spectrometer, and details are given in Supported Information. To obtain information on the molecular vibrational stretches, the frequency-shift method was used to eliminate the effect of the dielectric constant²².

- Lorraine, B., Ware, M. D., A., Michael, A. & Matthay, M. D. The Acute Respiratory Distress Syndrome. *N.Engl. Journal Med.* **342**, 1334–1349 (2000).
- Chin, C. D., Linder, V. & Sia, S. K. Lab-on-a-chip devices for global health: Past studies and future opportunities. *Lab Chip* **7**, 41–57 (2007).
- Erickson, D., Mandal, S., Yang, A. H. J. & Cordovez, B. Nanobiosensors: optofluidic, electrical and mechanical approaches to biomolecular detection at the nanoscale. *Microfluid Nanofluidics* **4**, 33–52 (2008).
- Hunt, H. K. & Armani, A. M. Label-free biological and chemical sensors. *Nanoscale* **2**, 1544–1559 (2010).
- Yan, R. *et al.* Label-free silicon photonic biosensor system with integrated detector array. *Lab Chip* **9**, 2163–2168 (2009).
- Monat, C., Domachuk, P. & Eggleton, B. J. Integrated Optofluidics: A New River of Light. *Nat. Photonics* **1**, 106–114 (2007).
- Pang, L., Chen, H. M., Freeman, L. M. & Fainman, Y. Optofluidic devices and applications in photonics, sensing and imaging. *Lab Chip* **12**, 3543–3551 (2012).
- Smolka, S., Barth, M. & Benson, O. Highly efficient fluorescence sensing with hollow core photonic crystal fibers. *Opt. Express* **15**, 12783–12791 (2007).
- Gong, J. Label-Free Attomolar Detection of Proteins Using Integrated Nanoelectronic and Electrokinetic Devices. *Small* **6**, 967–973 (2010).
- Homola, J. Surface Plasmon Resonance Sensors for Detection of Chemical and Biological Species. *Chem. Rev.* **108**, 462–493 (2008).
- Mock, J. J., Smith, D. R. & Schultz, S. Local Refractive Index Dependence of Plasmon Resonance Spectra from Individual Nanoparticles. *Nano Lett.* **3**, 485–491 (2003).
- Malima, A. *et al.* Highly sensitive microscale in vivo sensor enabled by electrophoretic assembly of nanoparticles for multiple biomarker detection. *Lab Chip* **12**, 4748–4754 (2012).
- Chen, Y. & Ming, H. Review of Surface Plasmon Resonance and Localized Surface Plasmon Resonance Sensor. *Photonic Sensors* **2**, 37–49 (2012).
- Jon, A. S. *et al.* Plasmonics for extreme light concentration and manipulation. *Nat. Mater.* **9**, 193–204 (2010).
- Ozbay, E. Plasmonics: Merging Photonics and Electronics at Nanoscale Dimensions. *Science* **311**, 189 (2006).
- Abbas, A., Linman, M. J. & Cheng, Q. New trends in instrumental design for surface plasmon resonance-based biosensors. *Biosensors and Bioelectronics*. **26**, 1815–1824 (2011).
- Chang, T. Y. *et al.* Large-scale plasmonic microarrays for label-free high-throughput screening. *Lab Chip* **11**, 3596–3602 (2011).
- Liu, Y. & Zhang, X. Metamaterials: a new frontier of science and technology. *Chem. Soc. Rev.* **40**, 2494–2507 (2011).
- Adato, R. *et al.* Ultra-sensitive vibrational spectroscopy of protein monolayers with plasmonic nanoantenna arrays. *Proc. Natl Acad. Sci. USA* **106**, 19227–19232 (2009).
- Nie, S. & Emory, S. R. Probing Single Molecules and Single Nanoparticles by Surface-Enhanced Raman Scattering. *Science* **275**, 1102–1106 (1997).
- Ataka, K. & Heberle, J. Biochemical Applications of Surface-Enhanced Infrared Absorption Spectroscopy. *Anal. Bioanal. Chem.* **388**, 47–54 (2007).
- Luk'Yanchuk, B. *et al.* The Fano resonance in plasmonic nanostructures and metamaterials. *Nat. Mater.* **9**, 707–715 (2010).
- Wu, C. *et al.* Fano-resonant asymmetric metamaterials for ultrasensitive spectroscopy and identification of molecular monolayers. *Nat. Mater.* **11**, 69–75 (2012).
- Watts, C. M., Liu, X. & Padilla, W. J. Metamaterial Electromagnetic Wave Absorbers. *Adv. Mater.* **24**, P98–P120 (2012).
- Fang, A., Koschny, T. & Soukoulis, C. M. Self-consistent calculations of loss-compensated fishnet metamaterials. *Phys. Rev. B*. **82**, 121102 (2010).
- Hao, J. *et al.* High performance optical absorber based on a plasmonic metamaterial. *Appl. Phys. Lett.* **96**, 251103–251104 (2010).
- Hao, J., Zhou, L. & Qiu, M. Nearly total absorption of light and heat generation by plasmonic metamaterials. *Phys. Rev. B*. **83**, 165107 (2011).
- Liu, X., Starr, T., Starr, A. F. & Padilla, W. J. Infrared Spatial and Frequency Selective Metamaterial with Near-Unity Absorbance. *Phys. Rev. Lett.* **104**, 207403 (2010).
- Landy, N. I., Sajuyigbe, S., Mock, J. J., Smith, D. R. & Padilla, W. J. Perfect Metamaterial Absorber. *Phys. Rev. Lett.* **100**, 207402 (2008).
- Yu, C., Ganjoo, A., Jain, H., Pantano, C. G. & Irudayaraj, J. Mid-IR Biosensor: Detection and Fingerprinting of Pathogens on Gold Island Functionalized Chalcogenide Films. *Anal. Chem.* **78**, 2500–2506 (2006).
- Chen, K., Adato, R. & Altug, H. Dual-Band Perfect Absorber for Multispectral Plasmon-Enhanced Infrared Spectroscopy. *ACS Nano*. **6**, 7998–8006 (2012).
- Liu, N. *et al.* Planar Metamaterial Analogue of Electromagnetically Induced Transparency for Plasmonic Sensing. *Nano Lett.* **10**, 1103–1107 (2010).
- Ding, P. *et al.* Dual-band perfect absorption and field enhancement by interaction between localized and propagating surface plasmons in optical metamaterials. *Journal of Optics* **13**, 75005 (2011).
- Harris, S. E. Electromagnetically Induced Transparency. *Phys. Today* **50**, 36–42 (1997).
- Jiang, Z. H., Yun, S., Toor, F., Werner, D. H. & Mayer, T. S. Conformal Dual-Band Near-Perfectly Absorbing Mid-Infrared Metamaterial Coating. *ACS Nano* **5**, 4641–4647 (2011).
- Nasse, M. J. *et al.* High-Resolution Fourier-Transform Infrared Chemical Imaging with Multiple Synchrotron Beams. *Nat. Methods* **8**, 413–416 (2011).
- Neubrech, F. *et al.* Resonant Plasmonic and Vibrational Coupling in a Tailored Nanoantenna for Infrared Detection. *Phys. Rev. Lett.* **101**, 157403 (2008).
- Malic, L., Veres, T. & Tabrizian, M. Nanostructured digital microfluidics for enhanced surface plasmon resonance imaging. *Biosensors and Bioelectronics*. **26**, 2053–2059 (2011).
- Soukoulis, C. M. & Wegener, M. Past achievements and future challenges in the development of three-dimensional photonic metamaterials. *Nat. Photonics* **5**, 523–530 (2011).
- Padilla, W. J. *et al.* Electrically resonant terahertz metamaterials: Theoretical and experimental investigations. *Phys. Rev. B*. **75**, 41102 (2007).
- Liu, N., Mesch, M., Weiss, T., Hentschel, M. & Giessen, H. Infrared Perfect Absorber and Its Application As Plasmonic Sensor. *Nano Lett.* **10**, 2342–2348 (2010).
- Feng, Q., Pu, M., Hu, C. & Luo, X. Engineering the dispersion of metamaterial surface for broadband infrared absorption. *Opt. Lett.* **37**, 2133–2135 (2012).
- Lu, B., Zheng, S., Quacha, B. Q. & Tai, Y. A study of the autofluorescence of parylene materials for mTAS applications. *Lab Chip* **10**, 1826–1834 (2010).
- Zhang, B. *et al.* Polarization-independent dual-band infrared perfect absorber based on a metal-dielectric-metal elliptical nanodisk array. *Opt. Express* **19**, 15221–15228 (2011).
- Li, T. *et al.* Surface-plasmon-induced optical magnetic response in perforated trilayer metamaterial. *Phys. Rev. E*. **76**, 16606 (2007).
- Papanikolaou, N. Optical properties of metallic nanoparticle arrays on a thin metallic film. *Phys. Rev. B*. **75**, 235426 (2007).
- Adato, R., Yanik, A. A. & Altug, H. On Chip Plasmonic Monopole Nano-Antennas and Circuits. *Nano Lett.* **11**, 5219–5226 (2011).
- Osawa, M., Ataka, K., Yoshii, K. & Nishikawa, Y. Surface-Enhanced Infrared Spectroscopy: The Origin of the Absorption Enhancement and Band Selection Rule in the Infrared Spectra of Molecules Adsorbed on Fine Metal Particles. *Appl. Spectrosc.* **47**, 1497–1502 (1993).
- Kneipp, K. *et al.* Single Molecule Detection Using Surface-Enhanced Raman Scattering (SERS). *Phys. Rev. Lett.* **78**, 1667–1670 (1997).
- Augie, B. & WL, B. Collective resonances in gold nanoparticle arrays. *Phys. Rev. Lett.* **101**, 143902 (2008).
- Piruska, A. *et al.* The autofluorescence of plastic materials and chips measured under laser irradiation. *Lab Chip*. **5**, 1348–1354 (2005).
- Sherry, L. J., Jin, R., Mirkin, C. A., Schatz, G. C. & Van Duyne, R. P. Localized Surface Plasmon Resonance Spectroscopy of Single Silver Triangular Nanoprisms. *Nano Lett.* **6**, 2060–2065 (2006).
- Mason, J. A., Allen, G., Podolskiy, V. A. & Wasserman, D. Strong Coupling of Molecular and Mid-Infrared Perfect Absorber Resonances. *IEEE Photonics Technol. Lett.* **24**, 31–33 (2012).
- Neubrech, F. *et al.* Resonant Plasmonic and Vibrational Coupling in a Tailored Nanoantenna for Infrared Detection. *Phys. Rev. Lett.* **101**, 157403 (2008).
- Dhindsa, M., Kuiper, S. & Heikenfeld, J. Reliable and low-voltage electro-wetting on thin parylene films. *Thin Solid Films* **519**, 3346–3351 (2011).

Acknowledgements

This work is financially supported in part by the National Science Foundation of China (NSFC-No.51175436), the Aeronautical Science Foundation of China (ASFC-No. 2012ZC53036), the Northwestern Polytechnical University Foundation for Fundamental Research (NPU-FFR-JC200811) and the 111 project from the Ministry of Education



(B13044). The authors thank Dr. Zhengwei Wu at the Institute of Electronics, Chinese Academy of Sciences (IECAS) and Baoqin Chen at the Institute of Microelectronics of the Chinese Academy of Sciences (IMECAS) for useful discussions and comments.

Author contributions

Y.L. and L.S. conceived the idea and designed the experiments. L.S. and C.S. performed the molecule measurements of Parylene C and data analysis. C.Y. helped to develop the absorption spectrum measurement. C.S. and J.D. prepared the Parylene C film. Y.F. provided advice on improving the experiments. Y.L. supervised the project and provided guidance and wrote the manuscript.

Additional information

Supplementary information accompanies this paper at <http://www.nature.com/scientificreports>

Competing financial interests: The authors declare no competing financial interests.

How to cite this article: Li, Y. *et al.* Surface-enhanced molecular spectroscopy (SEMS) based on perfect-absorber metamaterials in the mid-infrared. *Sci. Rep.* 3, 2865; DOI:10.1038/srep02865 (2013).



This work is licensed under a Creative Commons Attribution-NonCommercial-ShareAlike 3.0 Unported license. To view a copy of this license, visit <http://creativecommons.org/licenses/by-nc-sa/3.0>